

Effects of air damping on quality factors of different probes in tapping mode atomic force microscopy

Yu Zeng(曾瑜), Guo-Lin Liu(刘国林), Jin-Hao Liu(刘锦灏), and Zheng Wei(魏征)

Citation: Chin. Phys. B, 2024, 33 (**9**): 096806. DOI: 10.1088/1674-1056/ad5539
Journal homepage: http://cpb.iphy.ac.cn; http://iopscience.iop.org/cpb

What follows is a list of articles you may be interested in

Effects of Mg-doping temperature on the structural and electrical properties of nonpolar *a*-plane p-type GaN films

Kai Chen(陈凯), Jianguo Zhao(赵见国), Yu Ding(丁宇), Wenxiao Hu(胡文晓), Bin Liu(刘斌), Tao Tao(陶涛), Zhe Zhuang(庄喆), Yu Yan(严羽), Zili Xie(谢自力), Jianhua Chang(常建华), Rong Zhang(张荣), and Youliao Zheng(郑有炓)

Chin. Phys. B, 2024, 33 (**1**): 016801. DOI: 10.1088/1674-1056/acdc0b

Adsorption structure of macrocyclic energetic molecule DOATF on Au(111)

Xiao Chang(常霄), Li Huang(黄立), Yixuan Gao(高艺璇), Changjiang Yu(于长江), Yun Cao(曹云), Long Lv(吕龙), Xiao Lin(林晓), Shixuan Du(杜世萱), and Hong-Jun Gao(高鸿钧)

Chin. Phys. B, 2023, 32 (**9**): 096802. DOI: 10.1088/1674-1056/acda84

Theoretical and experimental study of phase optimization of tapping mode atomic force microscope

Zheng Wei(魏征), An-Jie Peng(彭安杰), Feng-Jiao Bin(宾凤姣), Ya-Xin Chen(陈亚鑫), and Rui Guan(关睿)

Chin. Phys. B, 2022, 31 (**7**): 076801. DOI: 10.1088/1674-1056/ac4a6d

NBN-doped nanographene embedded with five- and seven-membered rings on Au(111) surface

Huan Yang(杨欢), Yun Cao(曹云), Yixuan Gao(高艺璇), Yubin Fu(付钰彬), Li Huang(黄立), Junzhi Liu(刘俊治), Xinliang Feng(冯新亮), Shixuan Du(杜世萱), and Hong-Jun Gao(高鸿钧)

Chin. Phys. B, 2021, 30 (**5**): 056802. DOI: 10.1088/1674-1056/abeede

The properties of surface nanobubbles formed on different substrates

Zheng-Lei Zou(邹正磊), Nan-Nan Quan(权楠楠), Xing-Ya Wang(王兴亚), Shuo Wang(王硕), Li-Min Zhou(周利民), Jun Hu(胡钧), Li-Juan Zhang(张立娟), Ya-Ming Dong(董亚明)

Chin. Phys. B, 2018, 27 (**8**): 086803. DOI: 10.1088/1674-1056/27/8/086803

Effects of air damping on quality factors of different probes in tapping mode atomic force microscopy

Yu Zeng(曾瑜), Guo-Lin Liu(刘国林), Jin-Hao Liu(刘锦灏), and Zheng Wei(魏征)†

School of Mechanical and Electrical Engineering, Beijing University of Chemical Technology, Beijing 100029, *China*

(Received 10 April 2024; revised manuscript received 16 May 2024; accepted manuscript online 7 June 2024)

The AFM probe in tapping mode is a continuous process of energy dissipation, from moving away from to intermittent contact with the sample surfaces. At present, studies regarding the energy dissipation mechanism of this continuous process have only been reported sporadically, and there are no systematic explanations or experimental verifications of the energy dissipation mechanism in each stage of the continuous process. The quality factors can be used to characterize the energy dissipation in TM-AFM systems. In this study, the vibration model of the microcantilever beam was established, coupling the vibration and damping effects of the microcantilever beam. The quality factor of the vibrating microcantilever beam under damping was derived, and the air viscous damping when the probe is away from the sample and the air squeeze film damping when the probe is close to the sample were calculated. In addition, the mechanism of the damping effects of different shapes of probes at different tip–sample distances was analyzed. The accuracy of the theoretical simplified model was verified using both experimental and simulation methods. A clearer understanding of the kinetic characteristics and damping mechanism of the TM-AFM was achieved by examining the air damping dissipation mechanism of AFM probes in the tapping mode, which was very important for improving both the quality factor and the imaging quality of the TM-AFM system. This study's research findings also provided theoretical references and experimental methods for the future study of the energy dissipation mechanism of micro-nano-electromechanical systems.

Keywords: TM-AFM, quality factors, air viscous damping, air squeeze film damping

PACS: 68.37.Ps, 43.40.Cw, 46.40.Ff **DOI:** 10.1088/1674-1056/ad5539

1. Introduction

In 1986, Binning from IBM and Quate and Gerber from Stanford University jointly invented the atomic force microscope (AFM).[1] Since its introduction, AFM has become one of the most central tools for micro and nano research. It has become a fundamental tool for studying the properties of materials and surfaces at the micro and nano scale, and then performing micro and nano operations. Atomic force microscopy has three scanning modes:[2] Contact mode, tapping mode (TM-AFM), and non-contact mode. The tapping mode has the advantage of high imaging resolution while avoiding scratching and damage to the sample by the tip,[3] and has high application value in imaging soft, fragile, and highly adhesive materials.[4] At the same time, the tapping mode can obtain phase images along with morphological images, from which more information about a sample can be obtained than with morphological images alone,[5] such as the adhesion, elasticity, viscoelasticity, stiffness, and chemical structure of a sample surface. In TM-AFM, the phase images and quality factor are directly related to the energy dissipation of the system.[6] It has been determined that increasing the quality factor Q of the TM-AFM system can improve the imaging sensitivity and contribute to the resolution of the phase imaging.[7,8] In addition, the accurate identification of various energy dissipation mechanisms helps to further improve the accuracy of the imaging.

It has been demonstrated that the volume forces acting on an object, such as gravity and inertia forces, vary proportionally to the third power of the length. Meanwhile, surface forces, such as viscous forces, vary proportionally to the second power of the length. Therefore, as the size of an object continues to decrease, the surface forces on that object will gradually increase. At the microscale, the action of surface forces will have significant effects on the performance of an object.[9] Newell[10] first observed that air damping increases rapidly as the surface-mass ratio increases when a cantilever resonator is miniaturized and presented the formulas of quality factor at three different Knudsen numbers. In the atmospheric environment, the most significant surface force is the surrounding air damping force. For a micron-sized object vibrating near a surface, the air resistance mainly consists of air viscous damping force and air squeeze film damping force. When an object is vibrating away from the surface, the air squeeze film damping force tends to be very small and can be ignored, since the surface force mainly consists of air viscous damping force. However, when an object vibrates at a surface attachment, the air squeeze film damping force sharply increases as the gap in distance decreases, and the squeeze film damping force will not be negligible at that time.

Chen *et al.*[11] solved the energy dissipation of the system by considering the micro-cantilever beam as a cylinder of equal width and compared it with the experimental results. Sader *et al.*[12] developed a theoretical model of the energy dissipation of micro-cantilever beams under different excita-

†Corresponding author. E-mail: weizheng@mail.buct.edu.cn

© 2024 Chinese Physical Society and IOP Publishing Ltd

tion methods. Hosaka *et al.*[13] theoretically analyzed the damping characteristics of a beam resonator with transverse oscillations in order to estimate its energy dissipation and dynamic performance. The cantilever beam was considered to be a combination of several small spheres and an air viscous damping expression was obtained for the winding of the cantilever beam based on hydrodynamics.

As an object gradually approaches a surface, the air squeeze film effects become nonnegligible. At present,[9,14–17] studies regarding squeeze film damping mainly revolve around simple micro-electromechanical systems (MEMS),[14,18,19] such as squeeze film damping between parallel plates. However, there has been little discussion on the mechanism of action of squeeze film damping in TM-AFM. Pandey[20] presented an analysis of the errors between a one-dimensional simplified model of cantilever squeeze film damping and a two-dimensional (2D) model, which was very important in simplifying the Reynolds equation. In related theoretical studies,[21–24] many researchers have determined the effects of squeeze film damping on cantilever dynamics by solving the Reynolds equation, but have not considered the effects of different tip shapes on squeeze film damping.

As the tip–sample distance decreases, the air rarefaction effects are not negligible.[15,25,26] Previously, based on the analytical research of Fukui and Kaneko[27,28] in which the Boltzmann transport equation was adopted, Veijola *et al.*[29] obtained a simple approximate fit function for the effective viscosity coefficient, which was important for the calculation of air squeeze film damping under rarefied gas conditions.

The AFM probe in the tapping mode is a continuous energy dissipation process, from moving away from a sample to intermittent contact with a sample surface. At present, information regarding the energy dissipation mechanism of this continuous process is still sporadic in the relevant literature, and there are no systematic explanations or experimental verifications of the energy dissipation mechanism during each stage of the continuous process. Therefore, with the goals of furthering the understanding of the dynamics of TM-AFM and determining the mechanism of the damping action, this study carried out theoretical and simulated analyses, along with experimental verifications of the air damping dissipation mechanism of the continuous process of atomic force microscope probes with different shapes, from distances far away up to in contact with samples. The aforementioned research was considered to be important for reducing the background dissipation of TM-AFM and improving the phase imaging quality of AFM. The findings of this study also provide an important theoretical basis for MEMS/NEMS in order to reduce the energy dissipation and improve the quality factors of micro and nano resonators.

2. Theoretical analysis

2.1. Quality factor

The core component of TM-AFM is a micro-cantilever beam that is sensitive to weak forces. The force between the needle tip and a sample causes the micro-cantilever beam to change in vibration parameters, and the corresponding morphological and phase images are obtained by detecting such changes. It has been shown that the phase images of TM-AFM are reflections of the energy dissipation of the entire system,[25,28,30,31] where the dissipation of the adhesive contact between the tip and the sample is the key dissipation that reflects the properties of the sample. The total energy dissipation (the reciprocal of the quality factor, Q^{-1}) of the system can be written as follows:[7,32,33]

$$Q^{-1} = Q_{\mathrm{Key}}^{-1} + Q_{\mathrm{Bg}}^{-1} = Q_{\mathrm{Key}}^{-1} + Q_{\mathrm{vis}}^{-1} + Q_{\mathrm{sq}}^{-1} + Q_{\mathrm{bri}}^{-1} + \cdots, \quad (1)$$

where Q is the total system quality factor; Q_{Key}^{-1} is the adhesion contact dissipation (also referred to as the key dissipation between the tip and the sample), and Q_{Bg}^{-1} is the system background dissipation, Q_{vis}^{-1} is viscous dissipation, Q_{sqz}^{-1} is squeeze film dissipation, Q_{bri}^{-1} is liquid bridge dissipation.

Numerous studies.[28,30,31] indicate that phase image which was obtained in the TM-AFM scanning was not only controlled by the key dissipation between the tip and the sample, but the background dissipation also affected the phase image, where only the adhesive contact dissipation can reflect the nature of the sample. Meanwhile, a decrease in the contrast of the scanned image may be caused by the background dissipation, which could even potentially weaken mask, or distort (artifacts) the effective information in the phase image.[25,33,34] However, reducing the background dispersion of the TM-AFM can help to improve the micro-cantilever quality factor, which in turn can improve the quality of the phase image.[6,25,33–35] Typically, AFM operates in atmospheric environments where the background dissipation mainly consists of air damping dissipation.[7] Therefore, investigating the air damping dissipation mechanism in TM-AFM is of crucial significance for understanding phase imaging and enhancing phase contrast.

TM-AFM typically operates in the vicinity of the first natural frequency of the system, with information obtained by monitoring the displacement of the probe's free end. Therefore, a harmonic oscillator model can be utilized to depict the probe's motion, as shown in Fig. 1(b). The motion equation can be represented as

$$m_{\mathrm{e}}\ddot{z} + c_{\mathrm{e}}\dot{z} + k_{\mathrm{e}}(z - w) = F_{\mathrm{ts}}, \quad (2)$$

where z represents the absolute displacement of the probe tip, c_{e} represents the equivalent damping coefficient, m_{e} denotes the equivalent mass, and k_{e} stands for the equivalent stiffness. Furthermore, given $w(t) = B\sin\omega t$, where B represents the excitation amplitude, substituting into Eq. (2), we obtain

$$m_{\mathrm{e}}\ddot{z} + c_{\mathrm{e}}\dot{z} + k_{\mathrm{e}}z = B\sin\omega t + F_{\mathrm{ts}}. \quad (3)$$

Dividing both sides of the above equation by m_e, and neglecting the effect of the tip–sample force F_{ts}. Let $c_e/m_e = 2\xi\omega_0$, we arrive at the standard form

$$\ddot{z} + 2\xi\omega_0\dot{z} + \omega_0^2 z = \frac{B}{m_e}\sin\omega t, \tag{4}$$

where ω_0 is the first-order resonance frequency of the system, ξ is the total damping ratio of the system. Then, the amplification of the amplitude will be as follows:[15,26]

$$\beta(s) = \frac{1}{\sqrt{(1-s^2)^2 + (2\xi s)^2}}, \tag{5}$$

where $s = \omega/\omega_0$ represents the ratio of the excitation frequency to the resonance frequency in the tapping mode. Since the excitation frequency is generally comparable to the first-order resonance frequency, $s = 1 \pm \varepsilon$ can be applied, where ε is a small amount. The strong and weak nature of the damping system and the steepness of the resonance peak can be reflected by the amplification factor at resonance. At that time, the amplification factor at resonance is referred to as the quality factor and denoted as follows:

$$Q = \beta|_{s=1} = \frac{1}{2\xi}. \tag{6}$$

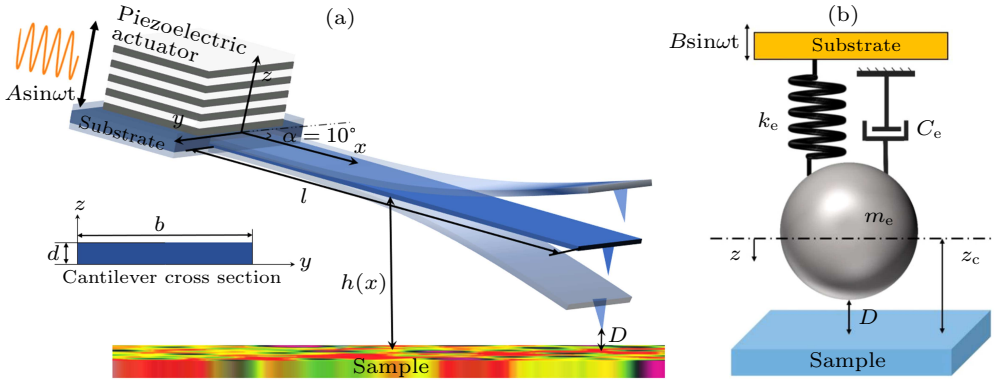


Fig. 1. (a) Illustration depicting the motion of a microcantilever beam under fixed-end displacement, (b) schematic diagram of a one-dimensional (1D) simplified spring-mass model for TM-AFM.

2.2. Dynamical model

When TM-AFM scans a sample, its excitation comes from the piezoelectric ceramic connected to the substrate. Based on this working principle, the differential equation of the free vibration of the Euler–Bernoulli beam evidently needs correction. Figure 1 illustrates a schematic diagram of the vibration with excitation present at the left end of the micro-cantilever beam, where $w(t)$ represents the excitation from the piezoelectric ceramic, which can also be expressed as $w(0,t)$. This model can be referred to as the CTS system (cantilever-tip–sample system, the CTS system). Therefore, the dynamical equations of the micro-cantilever can be described by the following equation:[25,34,36]

$$EI\frac{\partial^4[u(x,t)+w(t)]}{\partial x^4} + c_{\text{unit}}\frac{\partial[u(x,t)+w(t)]}{\partial t} + \rho bd\frac{\partial^2[u(x,t)+w(t)]}{\partial t^2} = F_{ts}\delta(x-l). \tag{7}$$

In the equation above, the second term on the left-hand side represents the damping force experienced by the system, where c_{unit} denotes the damping coefficient per unit length. It should be noted that most damping terms are not exactly proportional to velocity, but they can be equivalently obtained with respect to energy conservation; E and I are the Young's modulus and section moment of inertia of the microcantilever, respectively; l, b, and d represent the length, width, and thickness of the cantilever beam, respectively; F_{ts} represents the force between the tip and the sample. $\delta(x-l)$ is the Dirac delta function,[15,25,34,36] it is introduced as a concept of generalized functions to represent density distributions that are not continuously distributed in space or time, but rather concentrated at a single point or instant. In the theory of generalized functions, the exact meaning of the Dirac delta function should be understood in the context of integration. It can be defined as follows:

$$\delta(x-l) = \begin{cases} \infty, & x = l, \\ 0, & x \neq l, \end{cases} \quad \int_{-\infty}^{\infty}\delta(x-l)\,\mathrm{d}x = 1. \tag{8}$$

Assuming the excitation from the piezoelectric ceramic is a sinusoidal excitation, we have $w(t) = B\sin\omega t$, where ω is the excitation angular frequency. Substituting this into Eq. (7), we obtain

$$EI\frac{\partial^4 u(x,t)}{\partial x^4} + c_{\text{unit}}\frac{\partial u(x,t)}{\partial t} + \rho bd\frac{\partial^2 u(x,t)}{\partial t^2} = f + F_{ts}\delta(x-l), \tag{9}$$

where $f = \rho bdB\omega^2\sin\omega t - c_{\text{unit}}B\omega\cos\omega t$, it can be regarded as a uniformly distributed load acting on the entire microcantilever beam. To solve Eq. (7), the method of separation of variables is used, assuming

$$u(x,t) = \sum_{i=1}^{\infty}\varphi_i(x)\,q_i(t), \tag{10}$$

where $\varphi_i(x)$ is the i-th mode shape function and $q_i(t)$ is the i-th response function. Substituting Eq. (10) into Eq. (7), we

obtain

$$EI\sum_{i=1}^{\infty}\varphi_i''''q_i + c_{\text{unit}}\sum_{i=1}^{\infty}\varphi_i\dot{q}_i + \rho bd\sum_{i=1}^{\infty}\varphi_i\ddot{q}_i = f + F_{\text{ts}}\delta(x-l). \tag{11}$$

Furthermore, from Eqs. (10) and (7), it is known that $\varphi_i'''' = \beta_i^4\varphi_i$, where $\beta_i = \sqrt[4]{\rho bd\omega_i^2/EI}$. Substituting $\varphi_i'''' = \beta_i^4\varphi_i$ into Eq. (11), we obtain

$$\frac{EI}{\rho bd}\sum_{i=1}^{\infty}\beta_i^4\varphi_i q_i + \frac{c_{\text{unit}}}{\rho bd}\sum_{i=1}^{\infty}\varphi_i\dot{q}_i + \sum_{i=1}^{\infty}\varphi_i\ddot{q}_i = \frac{f}{\rho bd} + \frac{F_{\text{ts}}}{\rho bd}\delta(x-l), \tag{12}$$

from the orthogonality property of the modal functions, we can deduce

$$\int_0^l \varphi_i(x)\varphi_j(x)\,\mathrm{d}x = \begin{cases} 0, & i\neq j, \\ \psi_j, & i=j, \end{cases} \quad i,j = 1,2,3,\ldots, \tag{13}$$

where ψ_j represents the integral value of the orthogonal mode of the j-th order, by calculation, it is determined that $\psi_1 \approx l$. Multiplying both sides of Eq. (12) by $\varphi_j(x)$ and integrating over the interval [0, l], and considering only the first-order state $i = j = 1$, we obtain

$$\ddot{q}_1(t) + \frac{1}{\rho bd\psi_1}\int_0^l c_{\text{unit}}\varphi_1^2\,\mathrm{d}x\dot{q}_1(t) + \frac{EI}{\rho bd}\beta_1^4 q_1(t) = \frac{f}{\rho bd\psi_1}\int_0^l \varphi_1\,\mathrm{d}x + \frac{F_{\text{ts}}}{\rho bd\psi_1}\int_0^l \varphi_1\delta(x-l)\,\mathrm{d}x, \tag{14}$$

when we neglect the complex nonlinear interaction force between the tip and the sample, by comparing Eqs. (14) and (3), we can obtain the damping ratio ξ of the CTS system as

$$\xi = \frac{1}{2\rho bd\psi_1\omega_0}\int_0^l c_{\text{unit}}\varphi_1^2\,\mathrm{d}x. \tag{15}$$

Therefore, the expression for the quality factor of the CTS system is

$$Q_{\text{CTS}} = 1\Big/\left(\frac{1}{\rho bd\psi_1\omega_0}\int_0^l c_{\text{unit}}\varphi_1^2\,\mathrm{d}x\right). \tag{16}$$

In the above equation, c_{unit} represents the surface force dissipation per unit length of the microcantilever beam caused by the environment. Therefore, from the above equation, it is evident that only c_{unit} needs to be determined to obtain the quality factor of the CTS system.

2.3. Air viscosity damping in TM-AFM

In a vacuum environment, AFM systems can disregard the energy dissipation caused by viscous damping. However, the operational requirements of many biological material detection and physical sensing processes are limited to gas or liquid environments. Therefore, in the practical applications of AFM systems, air is the most common fluid environment, and the damping problem of gas environment at microscale is also the most concerning energy dissipation problem.[23,37–41]

(i) Intrinsic region gas damping characteristics

In the intrinsic region, the air pressure is extremely low and the energy dissipation of the AFM system is mainly due to other forms of energy dissipation. Therefore, this working environment can be approximated as a vacuum environment. The quality factor of the AFM system is maximum and relatively stable in this stage.

(ii) Molecular region gas damping characteristics

In the molecular region, as the pressure gradually increases, gas molecules begin to randomly collide with the probe and sample surfaces, and the interaction between gas molecules can be neglected. At this time, gas damping begins to affect the quality factor of the AFM system, and as the gas pressure gradually increases, the quality factor of the AFM system gradually decreases.

(iii) Viscous region gas damping characteristics

When the gas pressure increases to a certain level, the gas environment can be regarded as a viscous fluid, and gas molecules not only collide with the probe and sample surfaces but also constantly collide and escape internally. At this time, viscous damping takes a dominant role in the energy dissipation of the AFM system, and as the gas pressure gradually increases, the quality factor of the AFM system further decreases.

TM-AFM is generally operated under laboratory atmospheric conditions, and the gas damping on micro-cantilever beams is viscous gas damping. In addition, it is necessary to consider the scale effects of the gas medium. The dimensionless number (Knudsen number) can be utilized to determine the flow region in which the fluid is flowing as follows:

$$K_n = \frac{\lambda}{l_{\text{s}}}, \tag{17}$$

where l_{s} is the characteristic length and λ is the average free range of the gas molecules, which can be expressed by the following equation:

$$\lambda = \frac{1}{\sqrt{2}\pi q^2 n}, \tag{18}$$

where q represents the effective diameter of the molecule and n indicates the local molecular number density of the air. Therefore, according to the Knudsen number, the flow can be divided into the following four states: continuous flow ($K_n < 0.001$), slip flow ($0.001 < K_n < 0.1$), transition flow ($0.1 < K_n < 10$), and free molecular flow ($K_n > 10$).

The squeeze film effects of the probe can be ignored when the probe is far away from the sample, and only the viscous damping of the gas is considered. This stage is referred to as the isolation stage, during which the beam needs to be considered as an isolated object for air damping. Also, during the isolation stage, the Knudsen number of the gas, $K_n \ll 1$, along

with the gas flow, will be consistent with the continuity assumption. Another important dimensionless number for fluid flow is the Reynolds number (Re):

$$Re = \frac{\rho_a v l_s}{\mu}, \tag{19}$$

where ρ_a indicates the air density, usually taken as $\rho_a = 1.293$ kg/m^3, v is the fluid velocity vector, and μ refers to the dynamic viscosity coefficient of air, usually taken as $\mu = 19.8 \times 10^{-6}$. For common AFM system probes, the Reynolds number is generally much less than 1. Therefore, the air can be considered as a small Reynolds number fluid.

2.3.1. Examination of the air viscous damping of the micro-cantilever

As can be seen from the above-mentioned analyses, during the isolation stage, the small Reynolds number effects of the air need to be taken into consideration. This study divided the air viscous damping of the probe into the following two parts: Micro-cantilever and the tip of the probe. The air viscous damping of the micro-cantilever beam was first analyzed.

According to the string bead model introduced by Hosaka,[13] the micro-cantilever can be approximated as an infinite number of tiny spheres. Therefore, by solving the sphere bypassing problem according to the Stokes equation, the fluid bypassing damping coefficient per unit length subjected to the beam vibration can be obtained using the following equation:[13,26,42]

$$c_1 = 3\pi\mu. \tag{20}$$

However, due to the special nature of the high frequency motion of the probe, it is also necessary to consider the penetration depth α when the probe vibrates. For viscous fluids, when an object vibrates in the fluids, there will be a transverse wave that is consistent with the vibration speed of the object, which tends to decay exponentially as it moves away from the flat plate. The depth at which the amplitude decays to $1/\mathrm{e}$ of the original is defined as the penetration depth δ. The expression of the penetration depth δ can be written as follows:[26,42]

$$\delta = \sqrt{\frac{2\mu}{\rho_a \omega}}, \tag{21}$$

where ω is the angular frequency of the object vibration. Therefore, when the probe vibrates in the air, there will be a thin layer of spiny flow around the probe, and the air at a distance from the surface of the object is the potential flow. On this basis, if the probe micro-element located at x satisfies the probe size l of a magnitude much larger than the penetration depth δ, and the probe amplitude is much smaller than its size, the following applies:

$$l^2\omega \gg \delta, \quad A \ll l, \tag{22}$$

where A indicates the object vibration amplitude. Then, the micro-element vibration can be regarded as a high-frequency vibration. At that time, with the exception of the thin layer immediately above the surface of the probe, other parts of the air can be regarded as ideal fluid. In TM-AFM, the motion of the probe generally satisfies Eq. (22). Therefore, when considering the damping coefficient of the fluid to which the micro-cantilever is subjected in air, it is necessary to consider both the damping force of the bypass caused by the fluid bypassing phenomenon, and the damping force of the high-frequency vibration caused by the presence of cyclonic flow around the micro-cantilever. Then, according to the Stokes equation, the damping coefficient of the fluid viscosity per unit length of the beam during high frequency vibration can be obtained as follows:[26,42,43]

$$c_2 = \frac{3\pi b}{4}\sqrt{2\rho_a \mu \omega}. \tag{23}$$

The air viscous damping coefficient per unit length of the micro-cantilever can be obtained as[42,44]

$$c_{vis} = c_1 + c_2 = 3\pi\mu + \frac{3\pi b}{4}\sqrt{2\rho_a \mu \omega}. \tag{24}$$

Then, the quality factor under the air viscous damping of the micro-cantilever can be obtained using Eqs. (24) and (16) as follows:

$$Q_{vis} = 1 \Big/ \left(\frac{1}{\rho b d \psi_1 \omega_0} \int_0^l \left(3\pi\mu + \frac{3\pi b}{4}\sqrt{2\rho_a \mu \omega} \right) \varphi_1^2 \mathrm{d}x \right). \tag{25}$$

2.3.2. Examination of the air viscous damping of micro-sphere and conical probes

For microsphere and conical probes, which have spherical and conical tips attached to the free end of the microcantilever beam, they are also subject to the effect of air viscous damping. However, since they are located at the free end of the microcantilever beam, their motion can be considered one-dimensional. Therefore, the quality factor of air viscous damping dissipation for microsphere and conical tips can be directly calculated using the quality factor formula of the harmonic oscillator model. Thus, this paper divides the calculation of the quality factor of the probe into two parts: the quality factor of the microcantilever beam and the quality factor of the probe tip. Next, this paper will explore the mechanism of air viscous damping dissipation for microsphere and conical tips.

The operation of a micro-sphere probe shown in Fig. 2. As can be seen in the figure, for a sphere of radius R, doing 1D simple harmonic motion in air, the damping coefficient on the sphere in the fluid can be expressed by the following equation:[26,42,44]

$$c_{vis,1} = 6\pi\mu R + 3\pi R^2\sqrt{2\rho_a \mu \omega}. \tag{26}$$

The air viscous damping of the micro-cantilever beam can be expressed by Eq. (24). Therefore, the quality factor of the

micro-sphere probe by air viscous damping can be obtained as follows:

$$Q_{\mathrm{vis},1} = 1\Big/\left(\frac{1}{2\rho bd\psi_1\omega_0}\int_0^l\left(3\pi\mu+\frac{3\pi b}{4}\sqrt{2\rho_a\mu\omega}\right)\varphi_1^2\,\mathrm{d}x + \frac{6\pi\mu R+3\pi R^2\sqrt{2\rho_a\mu\omega}}{m_e\omega}\right). \tag{27}$$

The effects of the conical tip were ignored in this study due to the relatively small size of the conical tip when compared with that of the micro-cantilever beam. In addition, it was considered that the theoretical solution would be too difficult to obtain due to the complex boundary conditions of the conical tip. This study's assumptions were proven correct in the later simulations and experimental results. Therefore, the quality factor of the conical probe by air viscous damping was obtained as follows:

$$Q_{\mathrm{vis},2} = 1\Big/\left(\frac{1}{2\rho bd\psi_1\omega_0}\int_0^l\left(3\pi\mu+\frac{3\pi b}{4}\sqrt{2\rho_a\mu\omega}\right)\varphi_1^2\,\mathrm{d}x\right). \tag{28}$$

It was clear from the analysis results in the above sections that the air viscous damping of the micro-sphere and conical probes consisted of two parts, namely, the micro-cantilever and the tip of the probe. Therefore, it was very important to determine the strength of the contributions of the air viscous damping of those different parts to the reductions in the air viscous damping of the probe, as well as the improvement of the quality factor. The probe parameters shown in Table 2 were utilized in this study. The energy dissipation caused by the viscous damping effects of the air for the micro-cantilever and probe tip were separately obtained from the previous analysis results. For the conical probe, the air viscous damping at the tip of the conical needle was determined to be so small that it could be neglected. For the micro-sphere probe, the air viscous dissipation quality factors were comparable for the microcantilever beam and microsphere tip at 1930 and 1490, respectively, for a total quality factor of 842. Therefore, it was indicated that the micro-sphere probe was not the same as the conical probe, and the air viscous dissipation of the tip was not negligible.

2.4. Air squeeze film damping in TM-AFM

When a probe moves gradually closer to a sample, the air squeeze film damping effects cannot be ignored. This is referred to as the squeeze film stage. During the squeeze film stage, it is necessary to consider not only the air viscosity damping effects, but also the air squeeze damping effects between the probe and the sample. The squeeze film damping between different probes and samples were next analyzed in this study.

In most cases, the squeeze film damping is governed by a combination of viscous and inertial effects inside the fluid, but for the micron-sized micro-cantilever of TM-AFM, the inertial effects are usually negligible. In this study, the squeeze film effects between the probe and the sample was expressed by the well-known Reynolds equation[14]

$$\frac{\partial}{\partial x}\left(h^3P\frac{\partial P}{\partial x}\right)+\frac{\partial}{\partial y}(h^3P\frac{\partial P}{\partial y}) = 12\mu\frac{\partial(Ph)}{\partial t}. \tag{29}$$

The Reynolds equation assumes that the fluid is flowing in a continuous region. The important dimensionless number (Knudsen number) to generally used to determine the flow region in which the fluid is flowing, as discussed in detail in the previous section.

For a TM-AFM system, the Knudsen number usually ranges between 0.001 and 10. When the fluid is in the region of slip and transition flow, and the traditional Reynolds equation can no longer accurately describe the squeeze film effects, and the dynamic viscosity of the fluid needs to be modified to take into account the rarefaction effects of the gas. Veijola *et al.* successfully corrected the gas rarefaction effects by introducing the following fitting function for the effective dynamic viscosity, considered to be valid in the range of $0 < K_n \leq 880$:[29]

$$\mu_{\mathrm{eff}} = \frac{\mu}{1+9.638K_n^{1.159}}. \tag{30}$$

Another important dimensionless number associated with the Reynolds equation is the squeeze number σ[15]

$$\sigma = \frac{12\mu L^2\omega}{P_a h^2}, \tag{31}$$

where ω is the excitation frequency, L indicates the characteristic length, and h is the thickness of the squeeze film. The above nondimensional simplifications of the Reynolds equation are conducted under the condition of compressible fluid. Typically, air squeeze film damping exhibits both viscous and elastic effects. For instance, when two parallel plates undergo high-frequency relative motion, the fluid between them cannot dissipate rapidly enough. On one hand, this hinders the motion of the plates, known as the viscous effect. On the other hand, due to compressibility, elastic effects occur. The squeeze number (σ) can be used to determine viscous and elastic effects. When $\sigma < 1$, viscous effects dominate, and elastic effects can be neglected. Conversely, when $\sigma > 1$, the elastic effects of the fluid must be considered. In TM-AFM, the squeeze number σ is usually much smaller than 1. Therefore, the stiffness effects of the squeeze film are neglected in this study, and only its damping effects are considered. Based on the above analyses, equation (29) is simplified as follows:[13]

$$\frac{\partial}{\partial x}\left(h^3\frac{\partial P}{\partial x}\right)+\frac{\partial}{\partial y}\left(h^3\frac{\partial P}{\partial y}\right) = 12\mu_{\mathrm{eff}}\frac{\partial h}{\partial t}. \tag{32}$$

2.4.1. Examination of the squeeze film damping of an inclined micro-cantilever

In this section, the effects of the squeeze film damping of a micro-sphere probe and conical probe on the quality factor of the probes were analyzed. The operations of a micro-sphere probe and a conical probe, respectively, are schematically detailed in Fig. 2. In this study, it was considered that the squeeze film damping of the probe could be divided into two parts: Micro-cantilever and probe tip. Therefore, the squeeze film damping of the micro-cantilever required analysis prior to analyzing the micro-sphere and conical probes.

In a real AFM system, the micro-cantilever and the sample will exhibit an angle of approximately 10°. The distance between the micro-cantilever and the sample can be denoted by a function $h(x)$. Typically, the amplitude of the free end of the micro-cantilever is in the order of tens of nanometers, which is much smaller than the distance between the free end of the micro-cantilever and the sample at rest. Therefore, the effects of the micro-cantilever vibrations on $h(x)$ can be ignored, and $h(x)$ can be expressed as follows:

$$h(x) = D + (l - x)\sin\alpha, \tag{33}$$

where l is the length of the micro-cantilever; and D represents the distance of the free end of the micro-cantilever from the sample. When combined with the actual size of the cantilever, the aspect ratio will $X = b/l \approx 0.2$. According to the research conducted by Pandey,[20] the smaller the aspect ratio, the smaller the damping coefficient errors calculated by the 1D and 2D cantilever models. To simplify the calculation process, the Reynolds equation can be reduced to one dimension and equation (32) can be simplified to the following:

$$\frac{\partial}{\partial y}\left(h^3\frac{\partial P}{\partial y}\right) = 12\mu_{\text{eff}}\frac{\partial h}{\partial t}. \tag{34}$$

Then, by integrating the above equation along the width of the cantilever beam and bringing in the boundary conditions (when $y = \pm b/2$, $P = p_{\text{a}}$, when $y = 0$, $\partial P/\partial y = 0$), the distribution of the pressure along the width of the cantilever beam can be obtained using the following equation:

$$\Delta P = \left(\frac{6\mu_{\text{eff}}}{h^3(x)}y^2 - \frac{3b^2\mu_{\text{eff}}}{2h^3}\right)\frac{\mathrm{d}h}{\mathrm{d}t}. \tag{35}$$

The squeeze film force per unit length of the cantilever can be obtained by integrating the above equation

$$F_{\text{p}} = \int_{-2/b}^{2/b} -\frac{\partial P}{\partial y}\mathrm{d}y = \frac{\mu_{\text{eff}}b^3}{h^3(x)}\frac{\mathrm{d}h}{\mathrm{d}t}. \tag{36}$$

Then, from the equation of dynamic viscosity $c = F/v$, the damping coefficient of the air squeeze film per unit length of the micro-cantilever can be obtained as follows:

$$c_{\text{sq}} = \frac{\mu_{\text{eff}}b^3}{(D + (l - x)\sin\alpha)^3}. \tag{37}$$

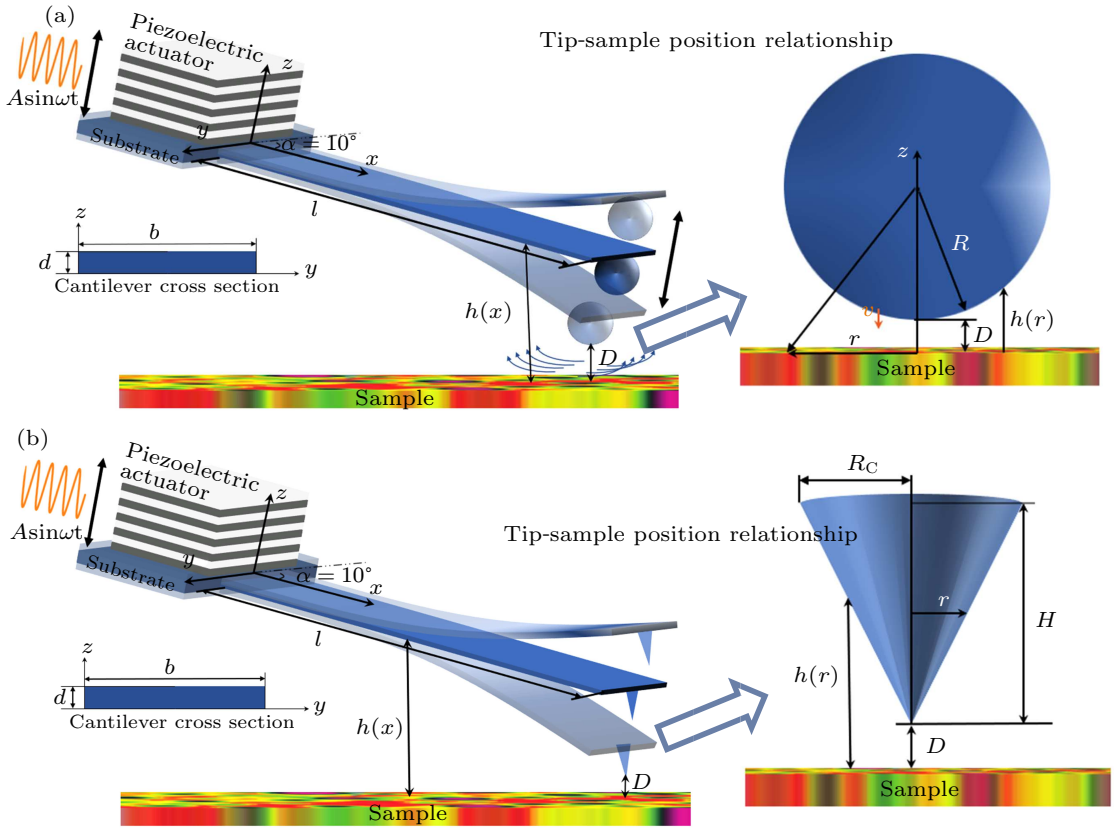


Fig. 2. Schematic diagrams of the operations of micro-sphere and conical probes: (a) micro-sphere probe, where $R = 15$ μm; (b) conical probe, where $R_{\text{C}} = 5$ μm, $H = 10$ μm.

2.4.2. Examination of the squeeze film damping of the micro-sphere and conical probes

In the previous section, we analyzed the air squeeze film damping effect on the microcantilever beam and derived the expression for the air squeeze film damping coefficient of the microcantilever beam. In this section, we will analyze the air squeeze film damping effect on the microsphere and conical tips, and derive the expressions for their air cushion damping coefficients.

As shown in Fig. 2, the spherical and conical surface squeeze film effects can be described by the Reynolds equation in cylindrical coordinates as follows:

$$12\mu_{\text{eff}}\frac{\partial h(r,t)}{\partial t}=\frac{1}{r}\frac{\partial}{\partial r}\left[rh^3(r,t)\frac{\partial p}{\partial r}\right]. \tag{38}$$

By letting $v=\mathrm{d}h/\mathrm{d}t$, the above equation can be integrated twice by r, and the expression for the pressure distribution can be obtained as follows:[15]

$$\Delta p=6\mu_{\text{eff}}v\int_r^R\frac{r}{h^3(r)}\,\mathrm{d}r, \tag{39}$$

where R is a value of r, which is assumed to be large enough to represent the farthest point in the region of the film layer. Then, based on that assumption, the total squeeze film force exerted by the fluid on the surface can be calculated using the following equation:

$$F_{\text{sq}}=\int_A\Delta p(n\cdot e_z)\,\mathrm{d}A. \tag{40}$$

As shown in Fig. 2(a), for the micro-sphere tip squeeze film effects, the film thickness can be approximated as follows:[45]

$$h(r)=D+\frac{R}{2}\left(\frac{r^2}{R^2}\right). \tag{41}$$

Then, by inserting Eq. (41) into Eqs. (39) and (40), the squeeze film damping coefficient of the micro-sphere tip can be calculated using the following equation:

$$c_{\text{sq},1}=\frac{6\pi\mu_{\text{eff}}R^2}{D}. \tag{42}$$

In the case of a real AFM probe, the free end of the microcantilever usually comes with a pyramidal tip. However, for a pyramidal structure, it is too difficult to solve theoretically. Therefore, in order to simplify the calculation, the pyramidal tip can be simplified to a conical tip as shown in Fig. 2(b). Then, for the conical tip squeeze film effects, the film thickness under the conical tip can be expressed in cylindrical coordinates as follows:

$$h(r)=D+2r. \tag{43}$$

Therefore, by inserting Eq. (43) into Eqs. (39) and (40), the squeeze film damping coefficient of the conical tip can be calculated using the following equation:

$$c_{\text{sq},2}=\frac{3\sqrt{5}\pi\mu_{\text{eff}}\left(3D(D+2R)^2(\log(D+2R)-\log(D))-2R\left(3D^2+9DR+4R^2\right)\right)}{8(D+2R)^2}. \tag{44}$$

In this study, based on the analysis results detailed in the above sections, it was clear that the squeeze film damping of the micro-sphere probe and the conical probe consisted of two parts, namely, the micro-cantilever and the tip of the probe. Therefore, it was very important to determine the strength of the contribution of the squeeze film damping of the different parts to the reduction of the squeeze film damping of the probe, as well as the improvement the quality factor. This study was able to obtain the curves of the variation of the squeeze film damping ratio with the tip–sample distances for the microcantilevers and the tips through the above theoretical analysis process, as detailed in Fig. 3.

As shown in Fig. 3(a), for the micro-sphere probe, the presence of the micro-meter sphere made the cantilever beam more than 30 μm away from the sample surface, resulting in the squeeze film damping mainly being concentrated on the micro-meter sphere. Since the squeeze film damping ratio of micrometer sphere was at least one order of magnitude larger than that of the micro-cantilever, the squeeze film damping of the micro-cantilever was no longer more important than that of the micro-meter sphere. In contrast to the microsphere probe, the micro-cantilever was subjected to a much larger squeeze film force than that of the conical tip, as shown in Fig. 3(b). In this study, it was believed that although the distance between the tip and the sample was much smaller than the distance between the micro-cantilever beam and the sample, the pressure film damping effects of the needle tip itself were small, leading to the pressure film damping being concentrated on the micro-cantilever beam. Therefore, the squeeze film damping of the micro-cantilever beam could be neglected for the micro-sphere probe, while the squeeze film damping of the conical tip could be neglected for the conical tip. Based on the above-mentioned results, this study was able to obtain the quality factor calculation equations for both the micro-sphere probe and the conical probe as follows:

$$Q_{\text{sq},1}=1\Big/\left(\frac{6\pi\mu_{\text{eff}}R_{\text{S}}^2}{Dm_{\text{e}}\omega_0}\right), \tag{45}$$

$$Q_{\text{sq},2}=1\Big/\left(\frac{\mu_{\text{eff}}b^3}{2\rho bd\psi_1\omega}\int_0^l\frac{\varphi_1^2}{\left(D+(l-x)\sin\alpha\right)^3}\,\mathrm{d}x\right), \tag{46}$$

where $m_e = 0.25m_{cantilever} + m_{tip}$, m_e is the equivalent mass of the probe,[25,34] $m_{cantilever}$ is the mass of the micro-cantilever, m_{tip} is the mass of the tip, $Q_{sq,1}$ is the quality factor of the micro-sphere probe, and $Q_{sq,2}$ is the quality factor of the conical probe.

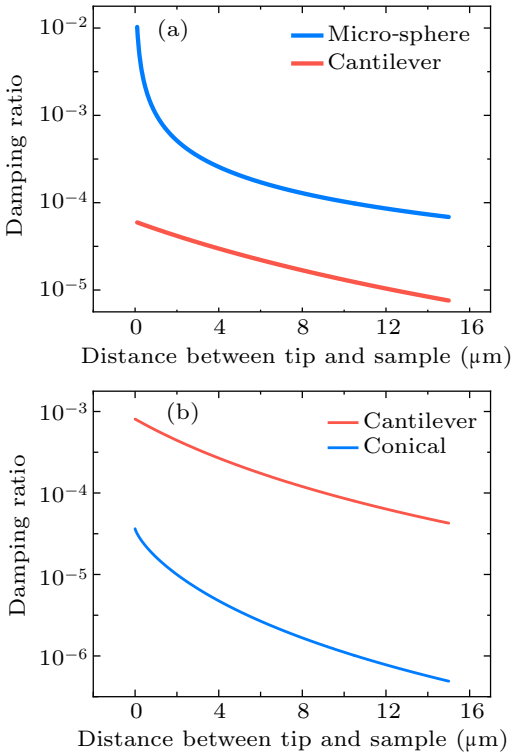


Fig. 3. Theoretical results of the squeeze film damping ratios for the different parts of the two examined probes: (a) squeeze film damping ratio of the micro-sphere probe; (b) squeeze film damping ratio of the conical probe. Note The parameters of the two types of probes are detailed in Table 2.

3. Simulation analysis

In this study, numerical simulations were used to calculate air viscous damping and squeeze film damping to further investigate the mechanism of the air damping action of the AFM probe. The simulation analysis results further confirmed the accuracy of the theoretical model.

3.1. Simulation models in COMSOL multiphysics

The interaction between the probe and the air is a fluid-structure coupling process. Since the dimensions of the probe are much smaller compared to the surrounding air domain, and its amplitude generally ranges only within a few tens of nanometers, the fluid motion induced by the probe vibration is considered to be a minor disturbance compared to the background flow field. Therefore, linearized Navier–Stokes (NS) equations can be used to describe the flow field. In this study, the finite element model of the probe in atmospheric conditions is established using the Thermal Viscous Acoustic (TVA) interface and the Pressure Acoustic (PA) interface available in the commercial finite element software package COMSOL Multiphysics. The TVA interface is used to solve the linearized Navier–Stokes equations, while the PA interface is used for the propagation of sound waves, with the outer boundary conditions terminating with spherical wave radiation conditions. Many studies have shown that these interfaces can accurately calculate the quality factors of microcantilever beam vibrations in atmospheric conditions.[46–52] Therefore, in this research, both the microcantilever beam and the sample substrate are modeled using solid mechanical elements, while the fluid around the probe is modeled using the TVA interface, and the fluid far from the probe is modeled using the PA interface. The finite element analysis software package COMSOL multiphysics implements the above physical interfaces through multi-physics coupling (acoustic–thermal boundary coupling and thermal–structural boundary coupling). As shown in Fig. 4, both the microcantilever and substrate are made of silicon, which with a density of 2329 kg/m^3, elastic modulus of 170 GPa, Poisson's ratio of 0.28, and the fluid domain is air.

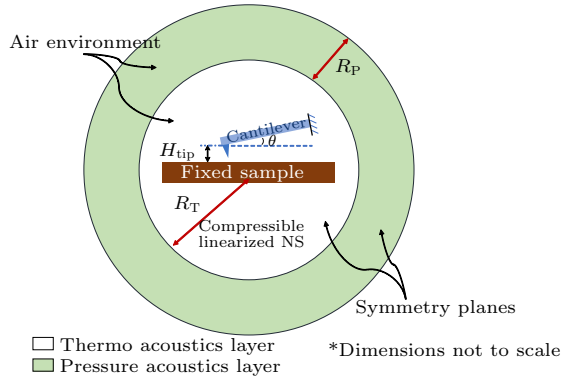


Fig. 4. Schematic representation of a three-dimensional finite element simulation model for a microcantilever probe immersed in an infinite fluid medium.

3.2. Results and discussion

As detailed in Table 1, the differences between the viscous dissipation quality factors of the two different probes obtained by theory and simulation were very small. The differences between the theory and simulation results were determined to be 8076 and 3038, respectively, which indicated that the theoretical models were more accurate. For the microsphere probes, the air viscous dissipation at the tip was not negligible. In addition, the air viscous dissipation quality factor of the probe was affected by both the micro-cantilever beam and the micro-sphere tip. In contrast, for the conical probes, it was determined that the air viscous dissipation at the probe tip could be neglected. To further analyze the distribution of air damping effects on the microcantilever beam and the probe tip, we used the finite element model shown in Fig. 4 to compute the pressure distribution around the microcantilever beam and the probe tip. To compare the pressure distribution for the microsphere and conical probes at varying distances from the tip to the sample, we extracted the pressure

data along the central axis of the probe and plotted the resulting graph as shown in Fig. 5.

Table 1. Comparisons of the theoretical and simulated viscous dissipation quality factors of a micro-sphere probe and a conical probe, where Q_{The} is the quality factor of probe from the theoretical calculations; Q_{Sim} is the quality factor from the numerical simulations, and $\Delta Q = |Q_{\mathrm{The}}^{-1} - Q_{\mathrm{Sim}}^{-1}|^{-1}$ is the quality factor differences between the simulation and experimental results.

	Micro-sphere probe	Conical probe
Q_{The}	842	458
Q_{Sim}	940	398
ΔQ	8076	3038

As shown in Fig. 5, the maximum pressures for both the micro-sphere probe and the conical probe were concentrated on the tip, and the pressure differences between the tip and the micro-cantilever gradually decreased as the tip–sample distance increased. For the microsphere probe, at a small tip–sample distance (for example, $D = 0.1$ μm), it was found that the pressure on the micro-sphere tip was more than four orders of magnitude greater than that on the micro-cantilever. However, for the conical probe, there was no significant difference observed between the pressure on the conical probe and the pressure on the micro-cantilever, with the exception of the tip of the conical, which generated a larger pressure. Therefore, it was concluded that for the micro-sphere probe, the squeeze film effects were concentrated on the micro-sphere tip, and for the conical probe, the squeeze film effects were distributed on the micro-cantilever, while the conical tip had little effect.

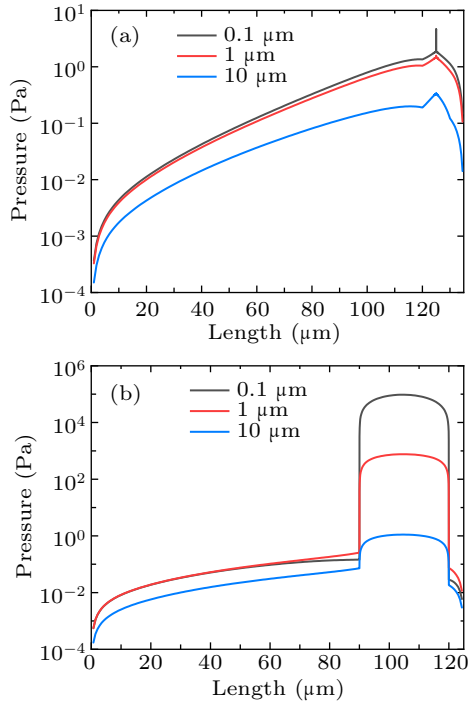


Fig. 5. Pressure distributions of a micro-sphere probe and a conical probe along the central axis of a micro-cantilever at different tip–sample distances: (a) micro-sphere probe, excited frequency $\omega/2\pi = 169$ kHz, amplitude $A = 50$ nm; (b) conical probe, excited frequency $\omega/2\pi = 268$ kHz, amplitude $A = 50$ nm.

Figure 6 details the total squeeze film forces on the micro-cantilever and the tips of both probes operating at different tip–sample distances. As can be clearly seen in the figure, in the case of the micro-sphere probe, the total squeeze force on the micro-sphere tip was more than two orders of magnitude greater than that on the micro-cantilever when the tip–sample distance was small (for example, $D = 0.1$ μm and $D = 1$ μm). However, when the tip–sample distance was greater (for example, $D = 10$ μm), the squeeze film force on both the micro-sphere tip and the micro-cantilever beam was minimal, and the squeeze effects of the probe were not obvious at that time. For the conical probe, it was observed that at different tip–sample distances (for example, $D = 0.1$ μm, 1 μm, and 10 μm), the total squeeze film force on the micro-cantilever was consistently much larger than that on the conical tip, which indicated that the squeeze film effects of the conical tip were very small compared with those of the micro-cantilever. Those findings were in good agreement with the results of the theoretical analysis described in the previous section.

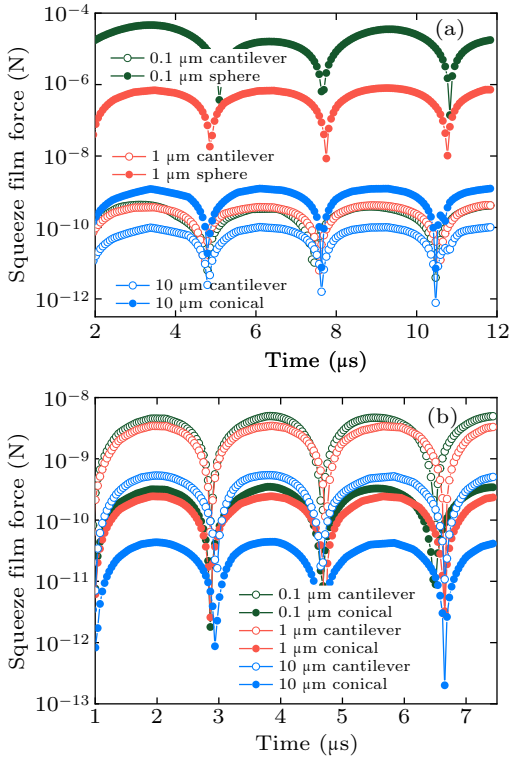


Fig. 6. Total squeeze film force on different parts of a micro-sphere probe and a conical probe at different tip–sample distances: (a) micro-sphere probe, excited frequency $\omega/2\pi = 169$ kHz, amplitude $A = 50$ nm; (b) conical probe, excited frequency $\omega/2\pi = 269$ kHz, amplitude $A = 50$ nm.

4. Experimental analysis

This study's frequency tune experiment was performed using a commercial AFM system (TM-AFM, Dimension 3100, Bruker). The initial use of the frequency tune experiment was to determine the resonance frequency of the micro-cantilever. In addition, the amplitude–frequency curve was obtained by varying the excitation frequency and obtaining the

frequency responses in order to obtain the quality factor of the system. When the probe was located far away from the sample, it was considered to be in the isolation stage, and the air squeeze film damping could be neglected. During that stage, the obtained amplitude–frequency curve tended to be stable and was directly related to the air viscous damping. Then, as the probe approached the sample, the air squeeze film damping was taken into consideration, and it was assumed that the differences in the amplitude–frequency curves at different distances were reflected in the frequency tune experiment. Therefore, to vary the tip–sample distance, the amplitude–frequency curves were obtained at each specific position using the tune and tip offset functions. The adjustable range of the tip offset for the experiment in this study was ±6.6 μm. For the conical probe, the tip–sample distance had been determined by the truncation of the amplitude–frequency curves. Truncation refers to the phenomenon where the amplitude significantly decreases due to the tip adhering to the sample when the tip–sample distance is sufficiently small (or when the tip is pressed into the sample).[15,34,35] In this study, we define the point of truncation on the amplitude–frequency curve as the point where the tip contacts the sample, which is when the tip–sample distance is zero microns. However, for the micro-cantilever beam and the microsphere probe, truncation does not occur, making it impossible to directly determine the absolute distance between the tip and the sample. Instead, only relative height variation can be observed. To obtain the absolute tip–sample distance, we fitted the Q–D curve of relative height variation with the theoretical Q–D curve, allowing us to deduce the absolute tip–sample distance.

During the experimental process, the half-power bandwidth of the system was obtained based on the amplitude–frequency curves. The quality factor was then estimated using $Q = \omega_0/\Delta\omega$, where $\Delta\omega$ is the bandwidth, and ω_0 is the first-order resonance frequency of the probe. Table 2 shows the detailed parameters of the three different types of probes.

In addition, the air viscous damping dissipation quality factor and the air squeeze film damping dissipation quality factor were simulated in COMSOL multiphysics, and the quality factors of the different probes at different tip–sample distances were obtained. The SEM images of three types of different probes are shown in Fig. 7.

Table 2. Basic parameters of the three different types of probes.

	Types	Elastic modulus (GPa)	Force constant (N/m)	Density (Si) (kg/m^3)	Resonance frequency (kHz)	Length (μm)	Width (μm)	Thickness (μm)	Tip size (μm)
Micro-cantilever	TL-NCH-10	190	68	2330	330	125	40	3.5	
Micro-sphere probe	TL-NCH-10	190	47	2330	167	125	40	3.5	$R = 15$
Conical probe	AN-NSC10-2	190	49	2330	268.5	135	30	3	$R_c = 5$ μm $H = 10$ μm

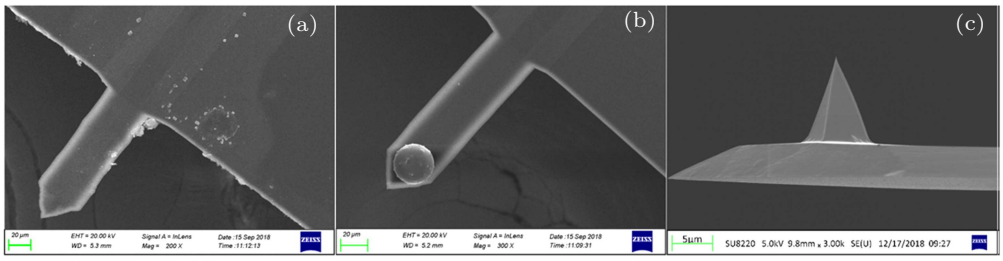


Fig. 7. SEM images of the three types of different probes: (a) micro-cantilever, (b) micro-sphere probe, (c) conical probe.

4.1. Results and discussion

As shown in Table 3, the difference between the experimental and the theoretical air viscous dissipation quality factor was found to be 1585 for the micro-cantilever beam when the probe was far away from the sample. This was considered to be the sum of the energy dissipation other than the air viscous dissipation. The experimentally obtained quality factor was 410. The comparison results showed that the air viscous dissipation was the dominant energy dissipation mechanism in the AFM system during the isolation stage. For the microsphere probe, the sum of the dissipation other than the air viscous dissipation was 2850, and for the conical probe, it was 2902. When compared with the experimental results, it was indicated that the same results were obtained for the micro-cantilever beam.

Table 3. Experimental, simulated, and theoretical air viscosity dissipation quality factors, where Q_{exp} is the quality factor obtained experimentally when the probe is away from the sample, Q_{sim} is the viscous dissipation quality factor obtained from the numerical simulations, Q_{the} is the viscous dissipation quality factor obtained from the theoretical calculations, ΔQ_1 is the quality factor difference between the simulation and experimental results; and ΔQ_2 is the quality factor difference between the theoretical and experimental results.

	Micro-cantilever	Micro sphere probe	Conical probe
Q_{exp}	410	650	350
Q_{sim}	553	940	398
Q_{the}	565	842	458
ΔQ_1	1585	2107	3038
ΔQ_2	1495	2850	1484

It was confirmed in this study that during the isolation stage, the air viscous dissipation was the most dominant energy dissipation mechanism in the AFM system. The discrepancies between theoretical, simulation, and experimental results are within a reasonable range, indicating that the theoretical and simulation models developed in this study can accurately describe the effects of air damping in TM-AFM to a certain extent.

As can be seen in the frequency–amplitude curves shown in Fig. 8, the quality factors of different probes were obtained at different tip–sample distances. In addition, to better compare the quality factors of different probes under different tip–sample distances obtained by theorical, experimental, and simulation methods, the theoretical, experimental, and simulation results were entered into one graph, as shown in Fig. 9.

As shown in Fig. 9(a), the tip–sample distance belonged to the squeeze film stage in the range of 0 to 16 μm, while above 16 μm, it belonged to the isolation stage. The quality factors and theoretical curves for the different tip–sample distances obtained from this study's simulations and experiments for the micro-cantilever beam were found to be in good agreement. This indicated that the theoretical simplified model was accurate and could be used to calculate the air damping dissipation of AFM probes. The quality factor shown in Fig. 9 represents the total quality factor of the TM-AFM system. The following analysis will focus primarily on the effect of air squeeze film damping on the quality factor. Therefore, the quality factor of air squeeze film damping dissipation in the subsequent analysis is obtained by subtracting the quality factor of air viscous damping dissipation from the total quality factor in Fig. 9.

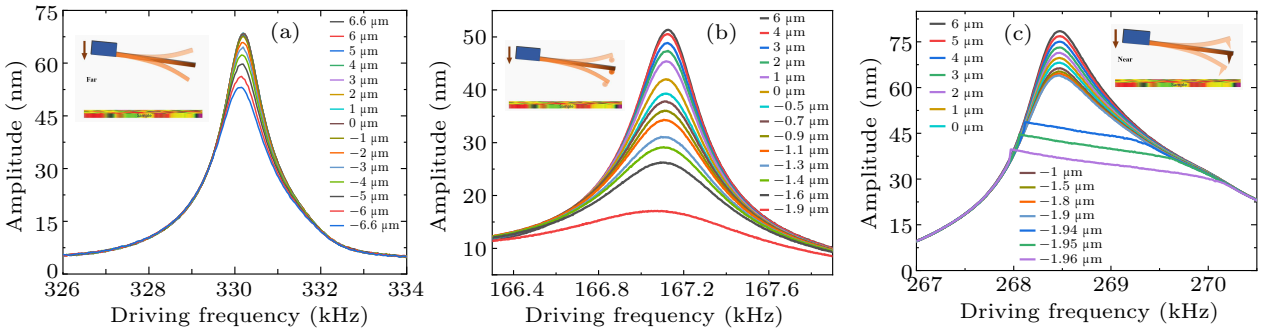


Fig. 8. Amplitude–frequency curves of the different probes at different positions: (a) micro-cantilever, (b) micro-sphere probe, (c) conical probe.

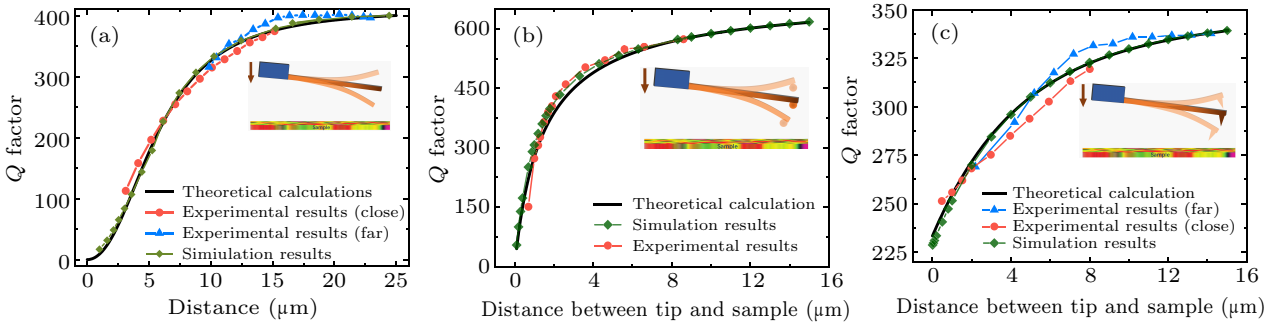


Fig. 9. Comparison of the theoretical calculations and the experimental and simulation results of the different probes: (a) micro-cantilever, where $Q_{\mathrm{vis}} = 410$; (b) micro-sphere probe, where $Q_{\mathrm{vis},1} = 650$; (c) conical probe, where $Q_{\mathrm{vis},2} = 350$; Q_{vis}, $Q_{\mathrm{vis},1}$, and $Q_{\mathrm{vis},2}$ are the air viscous dissipation quality factors, which were obtained experimentally when the probes were located far away from the sample.

As detailed in Fig. 9(a), the quality factor of the squeeze film damping dissipation was calculated to be 236 at a tip–sample distance of 5 μm. Meanwhile, this value was 1271 at a tip–sample distance of 10 μm and 2952 at a tip–sample distance of 15 μm. It can also be seen in the figure that the distances between the micro-cantilever beam and the sample had greatly affected the quality factor. For example, when the distance between the micro-cantilever beam and the sample was greater than 16 μm, the air squeeze film damping effects could be neglected.

Figure 9(b) illustrates that for the microsphere probe, the theoretical curve agreed well with the experimental and simulation results, which indicated that the air squeeze film damping of the micro-sphere probe had been concentrated on the micro-sphere tip. Those findings were consistent with this study's analytical results. At the same time, the presence of the micro-sphere tip greatly reduced the quality factor of the probe, which was calculated from the data displayed in Fig. 9(b). It was determined that the quality factor of the squeeze film damping dissipation was 461 when the tip–sample distance is 1 μm, and 1990 when the tip–sample distance was 4 μm, which indicated that the presence of the micro-sphere tip greatly reduced the quality factor when the tip–sample distance was very small.

As shown in Fig. 9(c), for the conical tip, the experimental and simulation results were in good agreement with the theoretical curve. Those results confirmed that it was reasonable that for the pyramidal tip to be simplified to a conical tip, and the squeeze film damping of the conical probe was concentrated on the micro-cantilever beam rather than on the probe tip. The squeeze film force on the conical tip was determined to be minimal and negligible. The squeeze film force on the micro-cantilever beam was inversely related to the distance between the micro-cantilever beam and the sample. Since the distance between the micro-cantilever beam and the sample consisted of two parts, the tip–sample distance and the height of the conical tip, it was believed in this study that increasing the height of the conical tip could effectively reduce the squeeze film damping effects and improve the quality factor.

As detailed in Fig. 9(c), it was found that the quality factor of the squeeze film damping dissipation was 715 when the tip–sample distance was 0 μm. However, that value was 5483 when the tip–sample distance was 10 μm. Since the conical tip was neglected, the increase of the tip–sample distance could be regarded as the increase of the conical tip height. Therefore, it was found that the quality factor of squeeze film damping dissipation was 715 when the conical tip height was 10 μm. When the conical tip height was 20 μm, that value was 5483, and at that time, the effects of the squeeze film damping on the quality factor of the AFM system could almost be ignored.

5. Conclusions

In this research study, the effects of air damping on the quality factor for micro-cantilever beam, micro-sphere probe, and conical probe were examined. When the probe was located a far distance from the sample, it was considered that the probe was in an isolation stage, during which the main energy dissipation mechanism was the viscous damping dissipation of the air. Then, when the probe was located closer to the sample, the probe entered a squeeze film stage, in which the air viscous damping and air squeeze film damping effects needed to be considered simultaneously. A new method was proposed in this study for calculating the equivalent viscous damping of micro-cantilever beams, by which the equivalent viscous damping considering air viscous damping and air squeeze film damping was calculated and compared with both the experimental and simulation results. The obtained results confirmed that the model was reasonable.

It is known that the mechanism of air damping action varies for probes with different tip shapes. During the isolation stage for the micro-sphere probe, the air viscous damping on the microsphere tip was comparable to that of the micro-cantilever beam. Conversely, for the conical probe, the air viscous damping on the conical tip was negligible. During the squeeze film stage, it was found that for the micro-sphere probe, the squeeze film damping of the probe was concentrated on the micro-sphere tip and the squeeze film damping of the microcantilever beam is negligible. In contrast, for the conical probe, the squeeze film damping of the conical tip was very small, the squeeze film damping of the probe was observed to be concentrated on the micro-cantilever beam. The squeeze film damping of the tip was considered to be negligible. Therefore, based on the above-mentioned results, this study believed that the squeeze film damping of the micro-sphere tip by the air was large. The quality factor of the micro-sphere probe was only a single-digit in the atmospheric environment when the tip–sample distance was very small, and it did not meet the requirements for accurately scanning samples. For the conical probe, the presence of the conical tip greatly increased the distance between the micro-cantilever beam and the sample, while the conical tip itself was subjected to very little air damping. It was determined that increasing the height of the probe tip could effectively reduce the squeeze film damping of the probe. Therefore, in the majority of the cases involving ordinary probes, when the tip height is above 20 μm, the squeeze film damping of the probe can be neglected.

In this study, a theoretical model for the air damping dissipation of different shapes of AFM probes at different stages was presented. In addition, it was verified through theory, experiments, and simulations that the air damping effects greatly reduced the quality factor of the system and affected the phase imaging quality of the TM-AFM. Such findings were considered to be very important for deepening the understanding of the air damping dissipation mechanism of AFM and improving the imaging quality of TM-AFM.

Acknowledgement

Project supported by the National Natural Science Foundation of China (Grant No. 11572031).

References

[1] Binnig G, Quate C F and Gerber C 1986 *Phys. Rev. Lett.* **56** 930
[2] Butt H-J, Cappella B and Kappl M 2005 *Surf. Sci. Rep.* **59** 1
[3] Hansma P K, Cleveland J P, Radmacher M, Walters D A, Hillner P E, Bezanilla M, Fritz M, Vie D, Hansma H G, Prater C B, Massie J, Fukunaga L, Gurley J and Elings V 1994 *Appl. Phys. Lett.* **64** 1738
[4] Miwa T, Yamaki M, Yoshimura H, Ebina S and Nagayama K 1995 *Langmuir* **11** 1711
[5] Stark R W, Drobek T and Heckl W M 1999 *Appl. Phys. Lett.* **74** 3296
[6] Tamayo J and García R 1998 *Appl. Phys. Lett.* **73** 2926
[7] Chen L W, Yu X C and Wang D 2007 *Ultramicroscopy* **107** 275
[8] Fairbairn M and Moheimani S O R 2013 *Rev. Sci. Instrum.* **84** 053706
[9] Bao M H and Yang H 2007 *Sens. Actuators, A* **136** 3
[10] Newell W E 1968 *Science* **161** 1320
[11] Chen G Y, Warmack R J, Thundat T, Allison D P and Huang A 1994 *Rev. Sci. Instrum.* **65** 2532
[12] Sader J E 1998 *J. Appl. Phys.* **84** 64
[13] Hosaka H, Itao K and Kuroda S 1995 *Sens. Actuators, A* **49** 87
[14] Han S, Ishfaque A, Phamduy P and Kim B 2020 *Microsyst. Technol.* **26** 1203
[15] Wei Z, Liu J, Zheng X T, Sun Y and Wei R H 2021 *J. Sound Vibrat.* **491** 115720

[16] Lin S M 2014 *Int. J. Mech. Sci.* **87** 26
[17] Zhao Y, Huang Q X, Zhang L S, Zhang Y and Cheng R J 2017 *Micromachines* **8** 226
[18] Lu C H, Li P and Fang Y M 2019 *Microsyst. Technol.* **25** 1753
[19] Wang W M, Tao F G, Wang Q, Qiu C K, Chen Z X and Fan B 2017 *Microsyst. Technol.* **23** 411
[20] Pandey A K and Pratap R 2007 *J. Micromech. Microeng.* **17** 2475
[21] Lee J W 2011 *J. Mech. Sci. Technol.* **25** 3005
[22] Mo Y M, Du L M, Qu B B, Peng B and Yang J 2018 *Microsyst. Technol.* **24** 1089
[23] Ostasevicius V, Dauksevicius R, Gaidys R and Palevicius A 2007 *J. Sound Vibrat.* **308** 660
[24] Syed W U, Brimmo A, Waheed O, Bojesomo A, Ali M H, Ocak I, Chengliang S, Chatterjee A and Elfadel I A M 2017 *J. Micromech. Microeng.* **27** 075016
[25] Wei Z, Liu J, Wei R H and Peng A J 2021 *J. Microsc.* **283** 219
[26] Kokubun K, Hirata M, Ono M, Murakami H and Toda Y 1987 *J. Vac. Sci. Technol., A* **5** 2450
[27] Fukui S and Kaneko R 1988 *J. Tribol.* **110** 253
[28] Bar G, Brandsch R, Bruch M, Delineau L and Whangbo M H 2000 *Surf Sci.* **444** L11
[29] Veijola T, Kuisma H, Lahdenperä J and Ryhänen T 1995 *Sens. Actuators, A* **48** 239
[30] Cleveland J P, Anczykowski B, Schmid A E and Elings V B 1998 *Appl. Phys. Lett.* **72** 2613
[31] Wei Z, Sun Y, Ding W X and Wang Z R 2016 *Sci. China: Phys., Mech. Astron.* **59** 694611
[32] Nayfeh A H and Younis M I 2003 *J. Micromech. Microeng.* **14** 170
[33] Liu G L, Zeng Y, Chen Y X and Wei Z 2024 *Acta Mech. Solida Sin.* **37** 297
[34] Wei Z, Peng A J, Bin F J, Chen Y X and Guan R 2022 *Chin. Phys. B* **31** 076801
[35] Garcıa R and Perez R 2002 *Surf. Sci. Rep.* **47** 197
[36] Kiracofe D and Raman A 2012 *Phys. Rev. B* **86** 205405
[37] Schmid S and Hierold C 2008 *J. Appl. Phys.* **104** 093516
[38] Mohanty P, Harrington D A, Ekinci K L, Yang Y T, Murphy M J and Roukes M L 2002 *Phys. Rev. B* **66** 085416
[39] Yakhot V and Colosqui C 2007 *J. Fluid Mech.* **586** 249
[40] Svitelskiy O, Sauer V, Liu N, Cheng K-M, Finley E, Freeman M R and Hiebert W K 2009 *Phys. Rev. Lett.* **103** 244501
[41] Imboden M and Mohanty P 2014 *Phys. Rep.* **534** 89
[42] Kokubun K, Hirata M, Ono M, Murakami H and Toda Y 1985 *J. Vac. Sci. Technol., A* **3** 2184
[43] Lévêque G, Girard P, Belaidi S and Cohen Solal G 1997 *Rev. Sci. Instrum.* **68** 4137
[44] Kim S, Kihm K D and Thundat T 2010 *Exp. Fluids* **48** 721
[45] Elsharkawy A A and AL-Fadhalah K J 2008 *Lubr. Sci.* **20** 61
[46] Liem A T, Ti C, Kara V, Ari A B, McDaniel J G and Ekinci K L 2021 *J. Appl. Phys.* **129** 064304
[47] Brar H S and Balantekin M 2020 *Meas. Sci. Technol.* **31** 095901
[48] Ricci A, Canavese G, Ferrante I, Marasso S L and Ricciardi C 2013 *Microfluid. Nanofluid.* **15** 275
[49] Mendez-Mendez J V, Alonso-Rasgado M T, Faria Correia E, Flores-Johnson E A and Snook R D 2014 *Micron* **66** 37
[50] Korayem A H, Abdi M and Korayem M H 2018 *Appl. Phys. A* **124** 417
[51] Korayem A H, Hafezi A and Abdi M 2019 *J. Braz. Soc. Mech. Sci. Eng.* **41** 520
[52] Sellier M, Lee Y C, Thompson H M and Gaskell P H 2009 *Comput. Fluids* **38** 171